Parallel Manipulator driven by Pneumatic Muscles

Salvador Sermeño Mena

Laboratoire Ampère (UMR 5005), INSA de Lyon, Université de Lyon, Villeurbanne, France
E-mail: salvador.sermeno-mena@ifd.mw.tu-dresden.de

Dr. Sylvie Sesmat

Laboratoire Ampère (UMR 5005), INSA de Lyon, Université de Lyon, Villeurbanne, France
E-mail: sylvie.sesmat@insa-lyon.fr

Professor Eric Bideaux

Laboratoire Ampère (UMR 5005), INSA de Lyon, Université de Lyon, Villeurbanne, France
E-mail: eric.bideaux@insa-lyon.fr

Abstract

Pneumatic muscles show severe parametric uncertainties and non linearities in the dynamic modeling. These uncertainties come mainly from air compressibility that cannot be neglected but also from the rubber stiffness of the muscle itself. Here FESTO™ pneumatic actuator muscles (PAM) are used for controlling the attitude of a platform with 2 degrees of freedom (DOF). This type of actuators has widely been used in robotic applications but usually the full operating range of the muscle is not used and the control is restricted to the part where the actuator characteristics are mostly linear. In this paper, we propose a complete dynamic model of this actuator, which consists in an extension of the usually used model determined by Daerden /3, 6/. It includes static as well as dynamic characteristics of the PAM, which have been validated experimentally. It shows that the mathematical model used in many papers in the literature are far from the real behavior of this type of component.

KEYWORDS: pneumatic actuator muscles, modeling, experimental characterization

1. Introduction

Pneumatic actuators, mainly cylinders, are widely used in robotics and automated systems due to their interesting volume to power ratio and also their low stiffness. This last characteristic makes them less dangerous while working with humans. In order for a robot to have a “human like” touch, there’s no need for a complex command, it’s simply needed that the actuators show some “compliance”. Pneumatic actuator muscle (PAM). PAMs are a flexible actuators that resemble the human muscle /1, 2, 3/. It is constituted by an inner tube with a braided sleeving. When the sleeves are filled by air the inner tube expands (the diameter increases) while the length decreases thus creating a traction force the long of the actuator (**Fig. 1**).

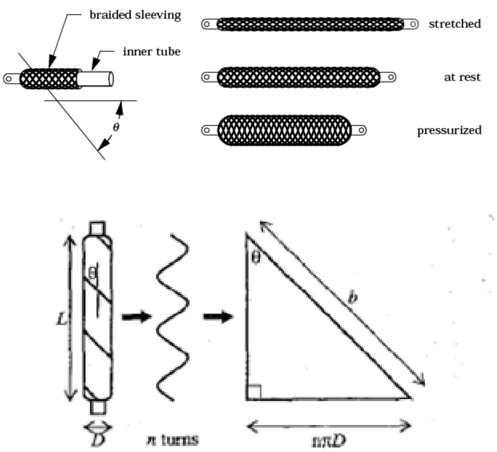

Figure 1: McKibben type muscle /3/.

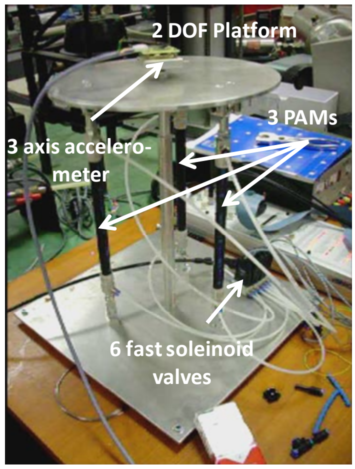

Figure 2: 2 DOF PAM platform.

The system under study (**Fig. 2**) is a platform with 2 DOF driven by 3 PAMs controlled by 6 fast solenoid 2/2 valves (2 per PAM: one for air supply / one for exhaust). The attitude (2 angles) is computed from accelerations provided by a 3-axis accelerometer. A fast prototyping system (DSpace) enables the data acquisition and the computation of the 6 valve commands according to the control scheme (**Fig. 3**). The platform is over-actuated (3 PAM for 2 DOF) and enables +/- 20° inclination in each direction.

Due to the non linearities, both in the mechanical part and in the PAM's behavior, the over-actuation that requires intelligent control allocation, and also because of the use of solenoid valves for driving the PAM's pressure, the attitude control of this platform shows many interests at the control level. Presently, in most research works /4, 5/, the PAMs are used in a limited domain; this enables the PAM to be considered nearly as a variable spring, and modeled as a bilinear form of pressure and contraction.

In order to enhance the control performances, the defined control architecture (Fig. 3) takes into account the main non linearities in the system. According to the two angular errors between the reference trajectory and the computed angles, the kinematic inverse model is used to decoupled the system and to determine the required forces on each PAM. Knowing the contractions (linked to the angular positions) and the desired force for each PAM, the required pressure to be controlled by the solenoid valves can be determined from the PAM inverse model. Whereas the inverse kinematic model is relatively easy to determine, the modeling of the PAM's static and dynamic characteristics requires a more complex approach. This is especially true if we want to maximize the range of use of this type of actuator in displacement magnitude and in frequency domain. The accuracy of modeling plays therefore a crucial role in the overall control performances.

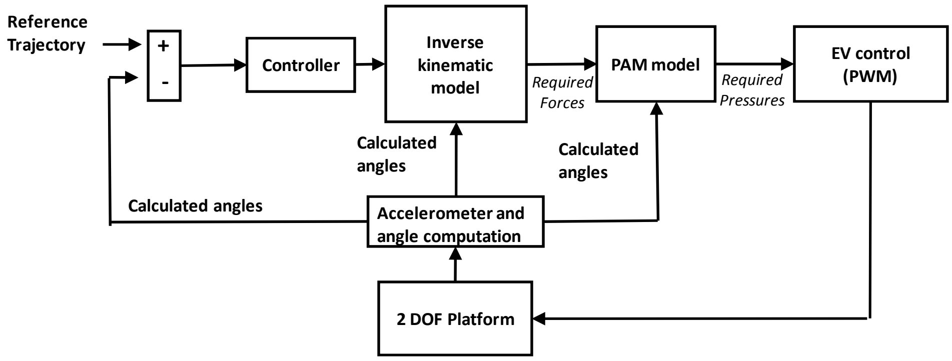

Figure 3: Control architecture.

We will not here focus on the control implementation, but the paper will aim at the muscle modeling and the experimental validation of different hypotheses. The static and dynamic models are firstly introduced. Then, experimental characterizations of the FESTO muscles are carried out and enable the identification of the PAM model. The validation of the model developed in LMS AMESim.Lab is finally presented.

2. PAM modelling

Using Daerden and Lefeber's research /3, 6/ we can obtain a theoretical model of the pneumatic muscle. The PAM transforms pneumatic power into mechanical power. A relationship between tension, length of the muscle and pressure has been determined using a theoretical approach.

2.1. PAM force modelling

Let's consider a muscle at a relative pressure P^*, an initial mass of air *dm* that enters the muscle. In *dt* seconds there's a volume change of *dV*. The muscle length changes in *dl.* We will neglect friction phenomena and the force needed to expand the tube. Work done by the gas is:

$$dW_{gas} = P^* dV \quad (1)$$

The amount of work produced by the muscle is:

$dW_{muscle} = -FdL,$ where F is the axial (contraction) force (2)

From the energy conservation law, $dW_{gaz} = dW_{muscle}$, consequently:

$$F = -P^* \frac{dV}{dL} \quad (3)$$

To estimate *dV/dL,* first it is assumed /3, 6/ the extensibility of the shell threads is very low, so the actuator volume will only depends on its length. In addition, the middle portion of the actuator is modeled as a perfect cylinder with zero-wall-thickness, where *L* is the length of the cylinder, θ **,** the angle between a braided thread and the cylinder long axis, *D,* the diameter of the cylinder, *n,* number of turns of a thread, and *b,* the thread length. *L* and *D* are expressed as functions of θ with constant parameters *n* and *b* (Fig 1)**.** The volume of the cylinder is then:

$$V(\varepsilon) = \frac{\pi}{4} D_0^2 l_0 (\frac{1}{sin^2\theta_0} - \frac{(1-\varepsilon)^2}{tan^2\theta_0})(1-\varepsilon) \tag{4}$$

Where D_0, is the diameter when θ equals 90°, l_0 the initial length of the muscle, ε is the contraction percentage of the muscle and θ_0 is the initial braided angle. Then *F* can be expressed as a function of P^* and ε by:

$$F(P^*, \varepsilon) = \frac{\pi}{4} D_0^2 * \left(\frac{3(1-\varepsilon)^2}{tan^2\theta_0} - \frac{1}{sin^2\theta_0}\right) P^* \tag{5}$$

In this approach, the contraction force is thus linearly proportional to the pressure, and is a monotonic function of the braid angle (0° < θ < 90°). In reality, the material extension is also contributing to the force and to the hysteretic form of the relation between force, contraction and pressure. To take into account these effects, an additional term, K(ε), has been considered for modeling the material stiffness. The second term has also been adjusted in order to improved the modeling of the equivalent section S(ε) according to the contraction ε as the mechanical work is not fully transformed in a contraction force. This lead to the following formulation:

$$F(\varepsilon, P^*) = S(\varepsilon)P^* + K(\varepsilon)\varepsilon \tag{6}$$

2.2. Pneumatic model

The PAM is a pneumatic chamber with a variable volume. According to Shearer /7/, we can establish a thermodynamic model using the first law of thermodynamics and mass conservation. The hypotheses considered for this approach are: air is a perfect gas, and, pressure, temperature and mass are homogeneous in the chamber. If a polytropic transformation is considered for the gas, the pressure dynamic in the PAM is given by:

$$\frac{dP}{dt} = \frac{1}{1+\frac{kP}{V(P,\varepsilon)}\frac{\delta V}{\delta P}}\left[-\frac{kP}{V(P,\varepsilon)}\frac{\delta V}{\delta \varepsilon}\frac{d\varepsilon}{dt} + \frac{krT}{V(P,\varepsilon)}(q_{ent} - q_{sort})\right] \tag{7}$$

This is the general form of the equation in which the volume of the chamber is dependent of the pressure and of its contraction.

3. Experimental characterization

Several experiments were carried out to characterize the muscle behavior in static and dynamic conditions in order to characterize force and volume according to pressure and contraction.

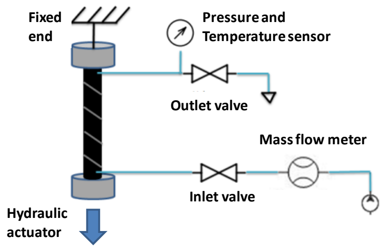

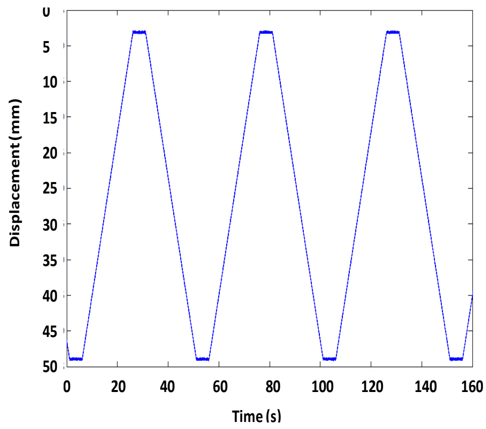

Figure 4: Experimental sketch

Figure 5: Displacement trajectory

With the muscle attached at one end to a fixed point and at the other end to a hydraulic actuator (**Fig. 4**), two types of tests have been carried out: fixed position and fixed pressure.

In fixed position tests, the PAM is slowly pressurized. The generated force, the pressure and the air mass flow rate can then be measured in quasi-static conditions.

In fixed pressure tests, the muscle is slowly deformed according to the controlled displacement (slow displacement ramp) of the hydraulic actuator (**Fig. 5**). Quasi-static displacement can be assumed as the used hydraulic actuator has very low friction and its control enables very slow and continuous displacements without steps. Contraction/expansion, generated force, and pressure can be measured in order to obtain contraction characteristics at fixed pressure.

3.1. Hysteretic phenomena

Fig. 6 shows the measurements obtained at a fixed pressure (5 bar), where the evolution of the generated force while contracting is in blue and in red while expanding. For comparison, the theoretical curve calculated using modified Daerden's model (eq. 10) and the Festo's data sheet characteristics at a given pressure are also shown. The difference between the generated force while contracting the muscle, and the generated force while expanding, it is around 60 N (the biggest gap). This hysteretic behaviour can be observed whatever the pressure is.

Because the observed hysteresis is low, the mean of both force characteristics (in contraction and in expansion) can be used for the following model identification procedures. However, this effect can be added a posteriori in the PAM's model.

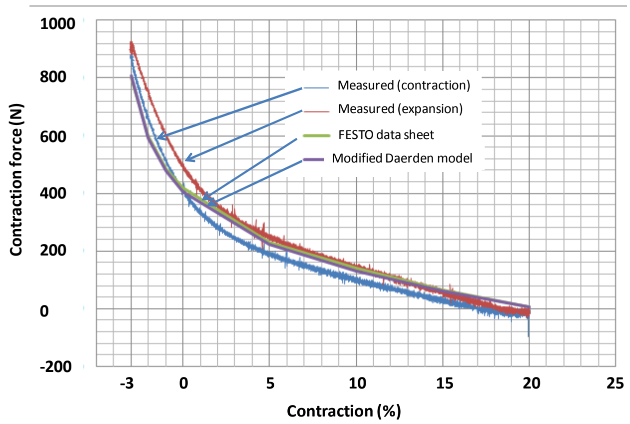

Figure 6: Hysteretic phenomena measured in quasi-static displacement at fixed pressure (5 bar).

3.2. PAM's contraction force.

In equation (7), the first term characterizes the mechanical work due to pressure and volume change (contraction), whereas the second term, the muscle stiffness, is only depending on the PAM's contraction.

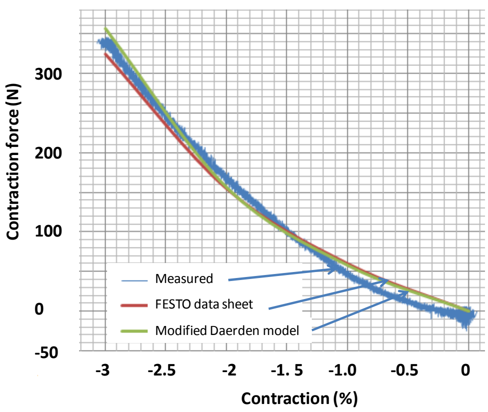

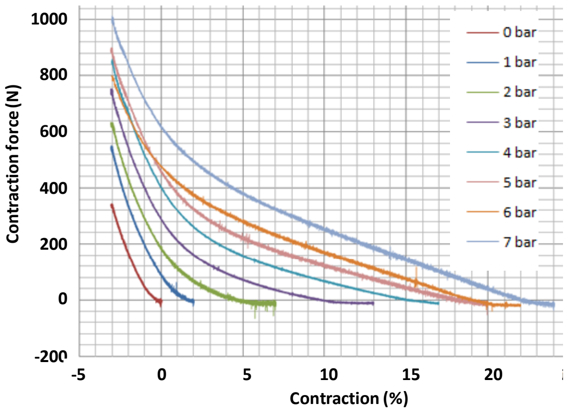

Figure 7: Contraction force at 0 bar. **Figure 8:** Measured contraction force

The muscle stiffness can be understood as an elastic force and it has been identified with traction measurements at 0 bar (relative pressure). In **Fig. 7**, the experimental results (in blue) show that this term has a high influence at low contraction or in expansion phases. It represents nearly half of the generated forces in this low expansion/contraction range. According to this measurement, the rubber stiffness is clearly non linear. It has a parabolic shape in the low expansion/contraction range, but is nearly zero when the contraction is high (**Fig.8**). Equation (8) enables to take into account this effect in the whole expansion/contraction domain:

$$K(\varepsilon) = A\frac{\varepsilon(\varepsilon - B_1)}{\varepsilon + B_2} \tag{8}$$

Figure 7 shows that the proposed modified Daerden's model in green (eq. 8) and the Festo’s characteristics (in red) are matching properly the experimental results (in blue)

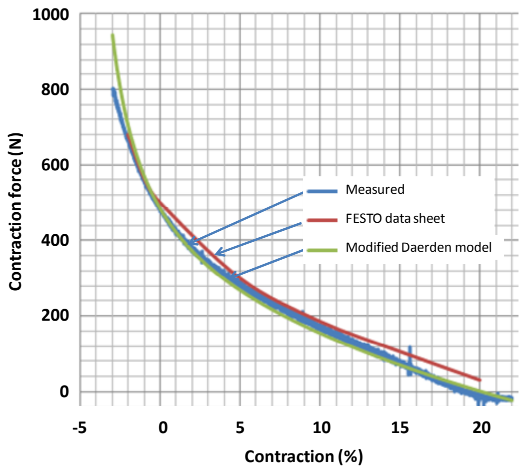

Figure 9: Equivalent section S(ε) at 6 barA.

The second term being identified, the first term of the equation can be determined from the mean of the expansion and contraction curves. Assuming a linear dependency on pressure, and a non linear (power form α) for contraction dependency, *S(ε)* is given by:

$$S(\varepsilon) = \frac{\pi}{4}D_0^2\left(\frac{3(1-\varepsilon)^a}{tan^2\theta_0} - \frac{1}{sin^2\theta_0}\right) \tag{9}$$

According to the results, at higher pressure we are able to match the theoretical and experimental values. However at low pressure and especially at low contraction, the error between both values is slightly larger.

Finally, the PAM's generated force can be approximated by the following expression:

$$F(P^*, \varepsilon) = \frac{\pi}{4}D_0^2\left(\frac{3(1-\varepsilon)^a}{tan^2\theta_0} - \frac{1}{sin^2\theta_0}\right)P^* + A\frac{\varepsilon(\varepsilon - B_1)}{\varepsilon + B_2} \tag{10}$$

3.3. PAM volume

The volume measurement is complex as the outer shape change is not necessarily representative of the inner volume change. In order to verify that the inner volume can be approximated by 3 discrete cylinders, which diameters change with contraction and pressure, and that the rubber thickness is nearly unchanged whatever the pressure is, 2 experimental procedures have been carried out. First, the muscle being set at a given contraction and pressure, the diameter is measured at 3 different points (**Fig. 10**). Second, the PAM being set initially at a given pressure, quasi-static contraction changes are applied and the pressure is measured in the closed volume.

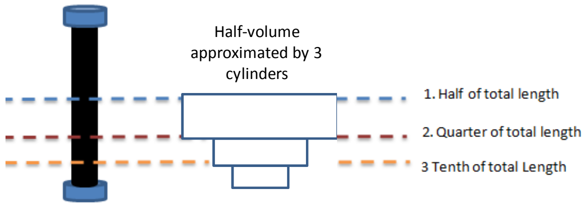

Figure 10: PAM's volume estimation

In the second procedure, we can assume for quasi-static transformation and no leakage, that $PV = cte$. Then, at initial state:

$$P_0 V_0 = cte \tag{11}$$

As the volume is closed, at a state i:

$$P_i V_i = P_0 V_0 \tag{12}$$

The volume V_i can though be deduced if the initial volume is accurately known:

$$V_i = V_0 \frac{P_0}{P_i} \tag{13}$$

From these 2 experimental procedures, it has been possible to measure accurately the real PAM's volume. It was firstly observed that the previous hypotheses can be verified.

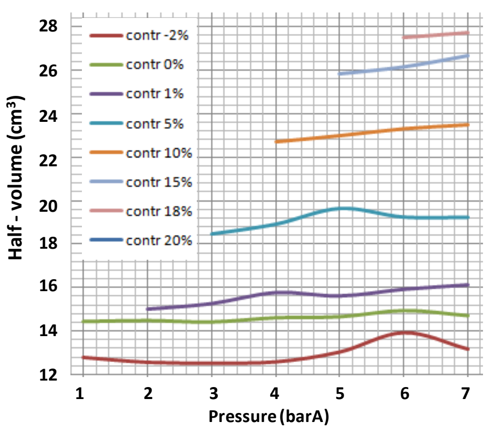

Figure 11: Volume vs pressure.

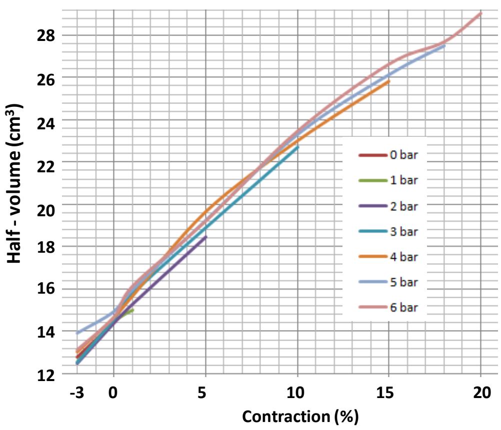

Figure 12: Volume vs contraction

Therefore, the volume can be approximated 3 discrete cylinders, which diameters and heights can be measured from outer diameter measurement and contraction as the rubber thickness is nearly unchanged whatever the pressure is.

Figure 11 shows that for a determined PAM contraction, the volume remains nearly unchanged with pressure. The influence of the PAM's contraction on volume change is illustrated on **Figure 12**. We can notice that the different measurements are close together, this validates furthermore the non-dependence of volume to pressure. These results show clearly that the volume change due to pressure can be neglected. Its influence is far less important than the contraction of the muscle.

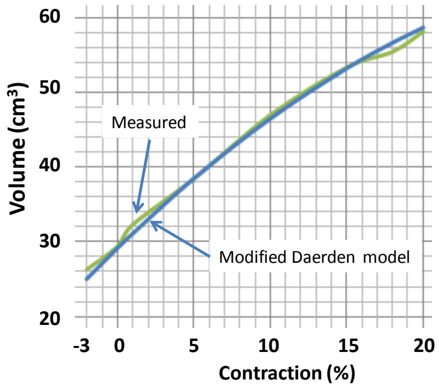

Figure 13: Volume vs contraction at 6 barA

Because the muscle contraction does not change with pressure, the muscle volume can be expressed as:

$$V(\varepsilon, P) = V(\varepsilon) \text{ and } \left(\frac{\delta V}{\delta P}\right)\Big|_{\varepsilon=cte} = 0 \tag{14}$$

Finally, to take into account the rubber deformation on the volume according to contraction, the Daerden model (eq. 5) has been modified in the same way as the equivalent section S(ε). The adjusted model (eq. 15) is matching properly the measurements at any pressure as shown on **Figure 13**.

$$V(\varepsilon) = \frac{\pi}{4} D_0^2 l_0 \left(\frac{1}{sin^2\theta_0} - \frac{(1-\varepsilon)^\alpha}{tan^2\theta_0}\right)(1-\varepsilon) \tag{15}$$

4. Simulation model and dynamic validation

Based on the previous parameter identification and hypotheses validation, the PAM model implemented in the LMS AMESim.Lab package is given by (16). Using the test rig described in Figure 4, several dynamic experiments were carried out and have allowed the validation of the proposed model nearly in the full operating range of the PAM. **Figure 14** shows the comparison of simulation and experimental results of one of these works. In this case, the hydraulic actuator applies to the PAM a sinusoidal displacement solicitation (Fig. 14a) and the PAM is connected to a pressure regulator. The displacement amplitude is defined in order to cover the maximum operating range of PAM at a given pressure.

$$\begin{cases} \frac{dP}{dt} = -\frac{kP}{V(\varepsilon)}\frac{\delta V}{\delta\varepsilon}\frac{d\varepsilon}{dt} + \frac{krT}{V(\varepsilon)}(q_{ent} - q_{sort}) \\ \frac{d\varepsilon}{dt} = \frac{1}{l_0}(u_1 - u_2) \\ V(\varepsilon) = \frac{\pi}{4}D_0^2 l_0\left(\frac{1}{sin^2\theta_0} - \frac{(1-\varepsilon)^\alpha}{tan^2\theta_0}\right)(1-\varepsilon) \\ F(\varepsilon, P) = \frac{\pi}{4}D_0^2\left(\frac{3(1-\varepsilon)^\alpha}{tan^2\theta_0} - \frac{1}{sin^2\theta_0}\right)(P - P_{atm}) + A\frac{\varepsilon(\varepsilon-B_1)}{\varepsilon+B_2} \end{cases} \tag{16}$$

The simulation model takes into account the PAM and the connecting circuit to the pressure regulator. The inputs for the simulation are the measured displacement and the regulator set pressure.

As the gain of the hydraulic actuator position control loop is low, the sinusoidal trajectory is not perfectly followed (Fig. 14a). In expansion mode (0 to -3% contraction), the parabolic part of the PAM stiffness (eq. 8) can be clearly observed. Figure 14b shows that the measured and simulated contraction forces are in good agreement in the full contraction range.

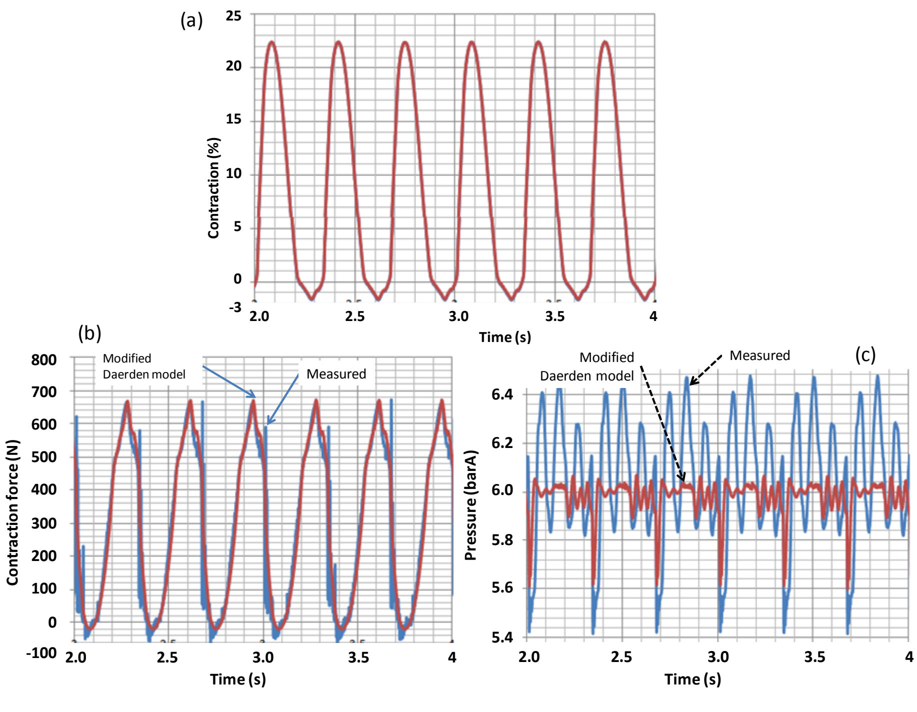

Figure 14: Model validation for sinusoidal solicitations at 3 hz and 6 barA

The results obtained for pressure in the PAM (Fig. 14c) are satisfying in contraction phases (from -3% to 20% contraction), but not in expansion phases (from 20% to -3%). Analyzing this problem, it has been observed that this effect is mainly due to the modeling of the pressure regulator considered in simulation as a perfect pressure source, which is not the case in reality. If the regulator outlet pressure is measured and used as input for the model, good results are obtained for the simulated PAM pressure.

Similar results have been obtained at low frequencies (up to 3 Hz), for other types of displacement trajectories (steps, …), and if the pressure is changed or varies slowly.

5. Conclusion and perspective

This experimental study has shown that the model usually used in the literature is far to be correct in the full operating range of PAM. Daerden's works /2,3/ were focused on McKibben muscles, which have a behavior different from the FESTO's PAM. For McKibben's, the muscle inflation is larger and the actuator stiffness has less influence on the muscle characteristic, but the contraction force is small compared to those obtained from the FESTO's PAM.

The proposed model leads to a real improvement of the simulation results without requiring very complex modeling effort. It has been shown that this model can be used for testing control laws in simulation in the full operating range of the PAM in static and dynamic conditions. At least but not last, the analytical formulation is enough simple to be used for non linear control synthesis. Present works look at extending this approach to other FESTO's PAM references (other lengths and sections) and at exploring the performances of the platform attitude control when the PAMs are used in their full operating range.

6. References

/1/ H. A. Baldwin, Realizable models of muscle function, Proceedings of the First Rock Biomechanics Symposium, pp. 139–148, New York, 1969.

/2/ J. Marcincin and A. Palko, Negative pressure artificial muscle—An unconventional drive of robotic and handling systems, Transactions of the University of Košice, pp. 350–354, Riecansky Science Publishing Co, Slovak Republic, 1993.

/3/ F. Daerden and D. Lefeber, The concept and design of pleated pneumatic artificial muscles, International Journal of Fluid Power, vol. 2, no. 3, pp. 41–50, 2001.

/4/ M. Girone, D. Burdea, M. Bouzit, V. Popescu, A Stewart Platform-Based system for Ankle Telerehabilitation, Autonomous Robots, 2001.

/5/ Xiaocong Zhu, Guoliang Tao, Bin Yao, and Jian Cao, Integrated Direct/Indirect Adaptive Robust Posture Trajectory Tracking Control of a Parallel Manipulator Driven by Pneumatic Muscles, IEEE Transaction on

Control System Technology, Vol. 17, No. 3, May 2009.

/6/ Frank Daerden et Dirk Lefeber, Pneumatic Artificial Muscles: actuators for robotic and automation, European journal of mechanical and environmental engineering, vol. 47, n°1, pp. 11-21, 2002.

/7/ J. L. Shearer, Study of pneumatic processes in the continuous control of motion with compressed air, Transactions of the ASME, vol. 78, pp. 233–242, 1956.

7. Symbols

P / P^*	absolute pressure / relative pressure	Pa
P_{atm}	atmospheric pressure	Pa
T	temperature	K
ε	muscle contraction	%
V	muscle volume	m^3
F	muscle contraction force	m^3
k	polytropic coefficient	
r	air constant	
q	mass flow rate (ent: inlet / sort: outlet)	kg/s
u	velocity	m/s
l_0	muscle free length	m
D_0	muscle free diameter	m
Θ_0	initial braided angle	rad
A, B_i, α	parameters	